


# Probabilistic distribution and stochastic *P*-bifurcation of a nonlinear energy-regenerative suspension system with time-delayed feedback control

Zhao-Bin Zeng(曾昭彬), Ya-Hui Sun(孙亚辉), and Yang Liu(刘洋)
**Citation:**Chin. Phys. B, 2026, 35 (**1**): 010201. DOI: 10.1088/1674-1056/ade669
http://cpb.iphy.ac.cn; http://iopscience.iop.org/cpb

**What follows is a list of articles you may be interested in**

---

## Adaptive multi-stable stochastic resonance assisted by neural network and physical supervision

Xucan Li(李栩灿), Deming Nie(聂德明), Ming Xu(徐明), and Kai Zhang(张凯)
Chin. Phys. B, 2025, 34 (**5**): 050203. DOI: 10.1088/1674-1056/adbd28

## Dynamic properties of rumor propagation model induced by Lévy noise on social networks

Ying Jing(景颖), Youguo Wang(王友国), Qiqing Zhai(翟其清), and Xianli Sun(孙先莉)
Chin. Phys. B, 2024, 33 (**9**): 090203. DOI: 10.1088/1674-1056/ad58c5

## A viscoelastic nonlinear energy sink with an electromagnetic energy harvester: Narrow-band random response

Zhi-Jing Liao(廖志晶), Ya-Hui Sun(孙亚辉), and Yang Liu(刘洋)
Chin. Phys. B, 2024, 33 (**7**): 070205. DOI: 10.1088/1674-1056/ad4632

## Performance enhancement of a viscoelastic bistable energy harvester using time-delayed feedback control

Mei-Ling Huang(黄美玲), Yong-Ge Yang(杨勇歌), and Yang Liu(刘洋)
Chin. Phys. B, 2024, 33 (**6**): 060203. DOI: 10.1088/1674-1056/ad3b89

## Stationary response of stochastic viscoelastic system with the right unilateral nonzero offset barrier impacts

Deli Wang(王德莉), Wei Xu(徐伟), Xudong Gu(谷旭东)
Chin. Phys. B, 2019, 28 (**1**): 010203. DOI: 10.1088/1674-1056/28/1/010203

---

# Probabilistic distribution and stochastic $P$-bifurcation of a nonlinear energy-regenerative suspension system with time-delayed feedback control

Zhao-Bin Zeng(曾昭彬)[1], Ya-Hui Sun(孙亚辉)[1,2,†], and Yang Liu(刘洋)[2,‡]

[1] *School of Mathematics and Statistics, Guangdong University of Technology, Guangzhou* 510520, *China*
[2] *Exeter Small-Scale Robotics Laboratory, Engineering Department, University of Exeter, North Park Road, Exeter, EX*4 4*QF, United Kingdom*

(Received 12 May 2025; revised manuscript received 15 June 2025; accepted manuscript online 20 June 2025)

Energy-regenerative suspension combined with piezoelectric and electromagnetic transduction has evolved into a core technological pathway in advancing automotive design paradigms. With the aim of improving energy harvesting performance, time-delayed feedback control is widely used in an energy-regenerative suspension system under different external disturbances in this paper. Meanwhile, limited research has addressed the stochastic dynamics of time-delayed nonlinear energy-regenerative suspension systems. Different from previous studies, this work studies the stochastic response and $P$-bifurcation of the nonlinear energy-regenerative suspension system with time-delayed feedback control. Firstly, an approximately equivalent dimension reduction system is established by the variable transformation method, and then the stationary probability density function of amplitude is obtained by the stochastic averaging method. Secondly, the precision of the method used in this work is verified by comparing the numerical solutions with the analytical results. Finally, based on the stationary probability density function, the influence of system parameters on stochastic $P$-bifurcation and the mean output power is discussed.

**Keywords:** energy-regenerative suspension, stochastic $P$-bifurcation, stochastic resonance, time-delayed feedback control

**PACS:** 02.30.Ks, 02.30.Jr, 02.50.–r, 02.60.Cb

**DOI:** 10.1088/1674-1056/ade669 **CSTR:** 32038.14.CPB.ade669

## 1. Introduction

With the rapid development of economy and automobile industry, cars have become a convenient means of personal transportation and have entered thousands of households. However, the explosive growth of automobiles has also brought a series of problems, such as huge energy consumption, serious waste of resources, and increased environmental pollution. About 10% to 16% of the fuel energy used to drive a vehicle is wasted due to road friction and thermal exhaust resistance,[1] and kinetic energy loss in suspension shock absorbers is one of the main energy consumption phenomena.[2] At the same time, vehicles on the road are subject to different disturbances, such as road irregularities, braking force, acceleration and centrifugal force on curved roads. These disturbances inevitably input external excitations to the car wheels, leading to vibrations of the whole body. This type of vibration not only increases additional energy consumption and causes damage to mechanical components, but also greatly affects driving comfort and stability. Especially for electric vehicles powered by battery packs, normal use can be compromised by bumping, extrusion, collision, and high temperature caused by vibration. This can reduce the service life and endurance of the battery, or cause serious safety accidents due to excessive temperature and fire.[3] Over the past 40 years, researchers have conducted extensive research on active and semi-active suspensions, showing improved vehicle dynamic performance at the cost of complexity and additional energy consumption.[4–6] However, reducing vehicle energy loss is necessary to improve fuel economy, reduce emissions, and meet the power needs of other systems.[7–9] From the point of view of actual demand, if vibration energy can be efficiently harvested and converted into electric energy while suppressing vibrations, not only can the dynamic performance of the suspension be guaranteed, but the on-board electronic equipment and battery pack can also be charged. This has significant application value in extending battery life, improving endurances, and many other aspects. Therefore, automotive suspension with energy regeneration will become an important development direction in the future.[10,11]

The vibration excitation of automobile suspension mainly comes from the complex road environment, so the road roughness is closely related to the vibration energy recovered by automobile suspension. Many researchers have carried out dynamic analysis and experiments on energy-regenerative suspension system under different excitation.[12–21] Zhang[22]

†Corresponding author. E-mail: sunyh@gdut.edu.cn
‡Corresponding author. E-mail: Y.Liu2@exeter.ac.uk

© 2026 Chinese Physical Society and IOP Publishing Ltd. All rights, including for text and data mining, AI training, and similar technologies, are reserved.

built a dynamic simulation model of the suspension system to test the average recoverable energy. Wang *et al.*[23] designed a new regenerative hydraulic shock absorber system. Under sinusoidal excitation of 1-Hz and 25-mm amplitude, the system achieved a recoverable power of 260 W with an efficiency of about 40%. Zou *et al.*[24] mainly focused on the modeling and compliance analysis of the 7-DOF vehicle suspension model integrating the energy recovery damper, and gave the characteristics of the system according to the parameter analysis under sinusoidal excitation. Using a predetermined excitation with a given frequency and amplitude is sufficient to evaluate the performance of the suspension system. However, the actual road surface may be random and variable, it is necessary to fully consider the actual road excitation to maintain good synchronous vibration suppression and energy harvesting of the system. Gaussian white noise is an ideal choice to simulate the road environment for vehicle excitation.

According to the different vibration-electric energy conversion mechanisms, the vibration energy harvesting technology used for automotive suspension is mainly piezoelectric[25] and electromagnetic.[26] The mechanism of piezoelectric vibration energy harvesting technology is based on the positive piezoelectric effect of piezoelectric materials to convert vibration energy into electric energy. Wang[27] proposed a piezoelectric sensor with high power and density to harvest vibration energy of spring suspension system. Zhao[28] designed and proposed a new piezoelectric harvester for vehicle suspension system by combining the piezoelectric power generation model, the rotor dynamics model and the traditional 2-DOF suspension model, and obtained a power of up to 332.4 W in the study. Xie *et al.*[29] researched a dual-mass piezoelectric rod collector used for vehicle suspension vibration energy recovery, and further discussed the influence of the width, speed and road roughness of the piezoelectric rod on the root mean square of power generation. Xiao *et al.*[30] investigated the practicability of integrating a piezoelectric energy harvester into a quarter-vehicle suspension model. Electromagnetic energy recovery shock absorbers are mainly divided into linear and rotating types. Kou[31] proposed a novel electromagnetic linear hybrid active suspension with integrated linear motor and solenoid valve shock absorber. Zuo *et al.*[32] used rare earth permanent magnets and high permeability magnetic rings to configure a four-phase linear electromagnetic shock absorber. The rotating electromagnetic energy recovery damper converts the linear vertical vibration into the rotating vibration of the generator and generates electrical energy based on a linear to rotating transmission mechanism. According to the motion conversion mechanism of shock absorber proposed in the public literature, the rotating structure is mainly divided into hydraulic type and mechanical type. Li *et al.*[33] proposed a hydraulic damper for simultaneous vibration suppression and energy recovery. The mechanical motion converter mainly includes rack and pinion, ball screw and their improved structure.[34–37] In recent years, with the aim of integrating the merits of different energy-harvesting shock absorber designs, the research community has turned its attention to compound regenerative damper technologies. Satpute *et al.*[38] investigated a hybrid energy-regenerative shock absorber system combining a linear electromagnetic generator with a hydraulic damper. Taghavifar[39] connected the hydraulic damper in parallel with the electromagnetic generator, and estimated through Monte Carlo simulation that the vehicle speed at 54 km/h could generate 48 W of electric energy.

Although the composite energy-regenerative suspension is beneficial to improve the performance of the system, it is not enough in terms of power consumption and system control. Compared with other control methods, time-delayed feedback control demonstrates dual benefits of enhancing system stability while effectively suppressing undesirable oscillations and limit cycles in dynamic systems.[40,41] The implementation of time-delay feedback control in nonlinear vibration systems demonstrates synergistic advantages for concurrent vibration management and energy harvesting optimization.[42–45] Jin[46] studied the dynamic behavior of the optimal speed model with time-delayed feedback control, and the proposed control strategy can effectively suppress traffic congestion and significantly enhance the stability of traffic flow. Zhang[47] demonstrated that the implementation of time-delayed feedback control in stochastic rotational environments can significantly improve energy harvesting performance. Owing to its superior control performance, time-delayed feedback control has found widespread application in vibration energy harvesting systems.[48,49]

In this paper, the probability distribution and *P*-bifurcation of a nonlinear energy-regenerative suspension system with time-delayed feedback control under Gaussian white noise excitation are studied. The rest of this paper is summarized as follows. Section 2 is devoted to the description of the system with model equation. In Section 3, the approximate stationary solution of the system is derived from using stochastic averaging method. Section 4 verifies the effectiveness of the proposed method and further discusses the influence of system parameters on *P*-bifurcation and mean power of the system. Finally, some finds are drawn in Section 5.

## 2. System setup and simplification

As shown in the Fig. 1, the dynamics model of the energy-regenerative suspension system for a quarter of a vehicle can be simplified to a single degree of freedom system coupled with electromagnetic and piezoelectric energy harvesting circuits. Nguyen and Fokou[50,51] found that damping strongly

affects frequency hopping in frequency sweep, so the nonlinear damping force model in the form of velocity and displacement polynomial is introduced to understand the vibration suppression and energy harvesting behavior of the suspension system under various working conditions. The governing equations of system can be given as follows:

$$\begin{aligned} &M\ddot{X}+(b_3X^4-b_2X^2-b_1)\dot{X}+kX+\alpha k'X^3\\ &+r_1\bar{I}+r_2\bar{V}=-M\ddot{X}_{\rm b},\\ &L\dot{\bar{I}}+(R_{\rm L}+R_{\rm I})\bar{I}=r_1\dot{X},\\ &C_{\rm p}\dot{\bar{V}}+\frac{\bar{V}}{R_V}=r_2\dot{X}, \end{aligned} \tag{1}$$

of which the relative displacement of mass $M$ is denoted by $X$, while $X_{\rm b}$ accounts for the stochastic displacement excitation originating from road surface irregularities. The system's stiffness characteristics are characterized by coefficients $k$ and $k'$. $b_1$, $b_2$, and $b_3$ are the damping coefficients. The electromagnetic component is characterized by several key parameters: $L$ for inductance, $\bar{I}$ representing output current, $R_{\rm I}$ denoting coil resistance, $R_{\rm L}$ as load resistance, and $r_1$ quantifying the linear electromechanical coupling coefficient. Four primary parameters are defined for the piezoelectric component: the capacitance is denoted by $C_{\rm p}$, the load resistance by $R_{\rm V}$, the output voltage by $\bar{V}$, and the electromechanical coupling coefficient by $r_2$.

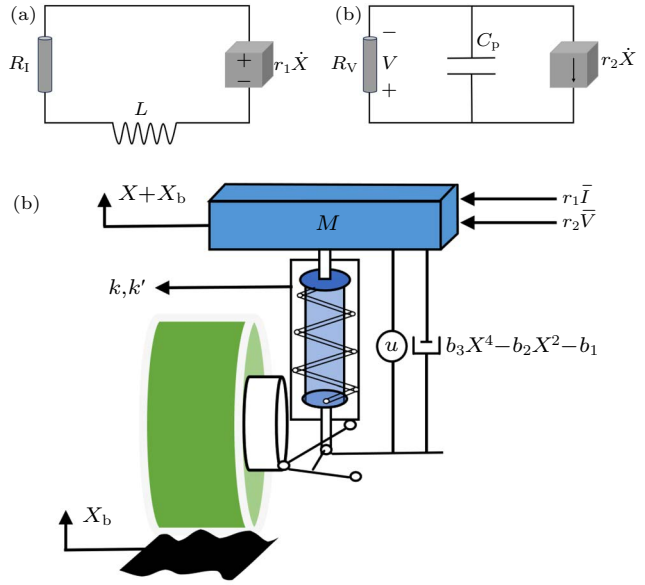



**Fig. 1.** (a) The equivalent circuit for electromagnetic element. (b) The equivalent circuit for piezoelectric element. (c) A quarter of nonlinear vehicle suspension with the time-delayed feedback control $u$.

Introduce the following dimensionless variables:

$$\begin{aligned} &\tau=\omega_0 t,\quad \omega_0=\sqrt{\frac{k}{M}},\\ &c_3=\frac{b_3}{M\omega_0},\quad c_2=\frac{b_2}{M\omega_0},\quad c_1=\frac{b_1}{M\omega_0},\\ &\varepsilon=\frac{\alpha k'}{k'},\quad \rho=\frac{r_1}{kL},\quad \mu=\frac{r_2}{kC_{\rm p}},\\ &\xi_1=\frac{R_{\rm L}+R_{\rm I}}{L\omega_0},\quad \eta_1=r_1,\quad \xi_2=\frac{1}{C_{\rm p}R_{\rm V}\omega_0},\quad \eta_2=r_2,\\ &V=C_{\rm p}\bar{V},\quad I=L\bar{I}. \end{aligned} \tag{2}$$

The coupled equations in dimensionless form are obtained as follows:

$$\begin{aligned} &\ddot{X}+(c_3X^4-c_2X^2-c_1)\dot{X}+X+\varepsilon X^3\\ &+\rho I+\mu V=-\ddot{X}_{\rm b}, &\text{(3a)}\\ &\dot{I}+\xi_1 I=\eta_1\dot{X}, &\text{(3b)}\\ &\dot{V}+\xi_2 V=\eta_2\dot{X}. &\text{(3c)} \end{aligned}$$

Here, letting $-\ddot{X}_{\rm b}=hw(t)$, $h$ denotes random excitation amplitude, and $w(t)$ represents Gaussian white noise with intensity $D$. Herein correlation function $E[w(t+l)w(t)]=2D\delta l$, $\delta(\cdot)$ is Dirac delta function.

By introducing time-delayed feedback control $u$, the mathematical equations for the energy-regenerative suspension system are formulated as follows:

$$\begin{aligned} &\ddot{X}+(c_3X^4-c_2X^2-c_1)\dot{X}+X+\varepsilon X^3\\ &+\rho I+\mu V+u=hw(t), &\text{(4a)}\\ &\dot{I}+\xi_1 I=\eta_1\dot{X}, &\text{(4b)}\\ &\dot{V}+\xi_2 V=\eta_2\dot{X}, &\text{(4c)}\\ &u=\lambda_1X_\tau+\lambda_2\dot{X}_\tau. &\text{(4d)} \end{aligned}$$

Compared with the system state, the initial phase $\theta$, frequency $\omega$, and displacement amplitude $A$ are all random slow processes. The system displacement and velocity by the generalized harmonic transformation[52–54] can be expressed as

$$\begin{cases} X(t)=A(t)\cos\varphi(t),\\ \dot{X}(t)=-A(t)\omega(A,\varphi)\sin\varphi(t),\\ \varphi(t)=\phi(t)+\theta(t),\\ \omega(A,\varphi)=\mathrm{d}\phi(t)/\mathrm{d}t. \end{cases} \tag{5}$$

Assume that the time delay $\tau$ is small enough, after harmonic transformation, the time delay terms $X_\tau$ and $\dot{X}_\tau$ can be approximated as

$$\begin{aligned} X(t-\tau) &\doteq A\cos[\omega(A,\varphi)(t-\tau)+\theta(t)]\\ &= X(t)\cos[\omega(A,\varphi)\tau]-\dot{X}(t)\frac{\sin[\omega(A,\varphi)\tau]}{\omega(A,\varphi)}, &\text{(6a)}\\ \dot{X}(t-\tau) &\doteq -A\omega(A,\varphi)\sin[\omega(A,\varphi)(t-\tau)+\theta(t)]\\ &= X(t)\omega(A,\varphi)\sin[\omega(A,\varphi)\tau]\\ &\quad+\dot{X}(t)\cos[\omega(A,\varphi)\tau]. &\text{(6b)} \end{aligned}$$

Equations (4b) and (4c) can be rewritten in the following form:[55]

$$\begin{aligned} I(t)&=Q_1(t)\,\mathrm{e}^{-\psi_1 t}+\int_0^t \mathrm{e}^{-\psi_1 t}\dot{X}(t_{\rm s})\,\mathrm{d}t_{\rm s},\\ V(t)&=Q_2(t)\,\mathrm{e}^{-\psi_2 t}+\int_0^t \mathrm{e}^{-\psi_2 t}\dot{X}(t_{\rm s})\,\mathrm{d}t_{\rm s}, \end{aligned} \tag{7}$$

where $Q_1(t)\mathrm{e}^{-\psi_1 t}$ and $Q_2(t)\mathrm{e}^{-\psi_2 t}$ are exponential decay terms with negligible effects on the stationary response. Using integration by parts and the transformation of variables $s = t - t_s$, equation (7) can be approximated as

$$\begin{aligned} I(t) &\doteq \int_0^t \mathrm{e}^{-\psi_1 t}\dot{X}(t-s)\,\mathrm{d}s, \\ V(t) &\doteq \int_0^t \mathrm{e}^{-\psi_2 t}\dot{X}(t-s)\,\mathrm{d}s. \end{aligned} \tag{8}$$

According to Eq. (6(b)), $\dot{X}(t-s)$ can be approximated by

$$\begin{aligned} \dot{X}(t-s) \doteq\ & X(t)\omega(A,\varphi)\sin[\omega(A,\varphi)s] \\ & +\dot{X}(t)\cos[\omega(A,\varphi)s]. \end{aligned} \tag{9}$$

Substituting Eq. (9) into Eq. (8), we can obtain

$$\begin{aligned} I(t) &\doteq \frac{A\eta_1\omega}{{\xi_1}^2+\omega^2}[\omega\cos\varphi-\xi_1\sin\varphi] \\ &= \frac{\eta_1\omega^2}{{\xi_1}^2+\omega^2}X+\frac{\eta_1\xi_1}{{\xi_1}^2+\omega^2}\dot{X}, \end{aligned} \tag{10a}$$

$$\begin{aligned} V(t) &\doteq \frac{A\eta_2\omega}{{\xi_2}^2+\omega^2}[\omega\cos\varphi-\xi_2\sin\varphi] \\ &= \frac{\eta_2\omega^2}{{\xi_2}^2+\omega^2}X+\frac{\eta_2\xi_2}{{\xi_2}^2+\omega^2}\dot{X}. \end{aligned} \tag{10b}$$

Owing to $\omega\cos\varphi-\xi_1\sin\varphi = \sqrt{{\xi_1}^2+\omega^2}\cos(\varphi+\tan^{-1}\frac{\xi_1}{\omega})$, equations (10a) and (10b) can be rewritten as

$$\begin{aligned} I(t) &\doteq \frac{A\eta_1\omega}{{\xi_1}^2+\omega^2}[\omega\cos\varphi-\xi_1\sin\varphi] \\ &= \frac{A\eta_1\omega}{\sqrt{{\xi_1}^2+\omega^2}}\cos\left[\varphi+\tan^{-1}\frac{\xi_1}{\omega}\right], \end{aligned} \tag{11a}$$

$$\begin{aligned} V(t) &\doteq \frac{A\eta_2\omega}{{\xi_2}^2+\omega^2}[\omega\cos\varphi-\xi_2\sin\varphi] \\ &= \frac{A\eta_2\omega}{\sqrt{{\xi_2}^2+\omega^2}}\cos\left[\varphi+\tan^{-1}\frac{\xi_2}{\omega}\right]. \end{aligned} \tag{11b}$$

Substituting Eqs. (6), (6b), (10a), and (10b) into Eq. (4a) leads to the following equivalent uncoupled mechanical equation:

$$\begin{aligned} &\ddot{X}+(c_3X^4-c_2X^2-c_1+u_2+d_2)\dot{X} \\ &+(1+u_1+d_1)X+\varepsilon X^3 = hw(t), \end{aligned} \tag{12}$$

where

$$\begin{aligned} u_1 &= \lambda_1\cos(\omega\tau)+\lambda_2\omega\sin(\omega\tau), \\ u_2 &= \lambda_2\cos(\omega\tau)-\frac{\lambda_1\sin(\omega\tau)}{\omega}, \\ d_1 &= \frac{\rho\eta_1\omega^2}{{\xi_1}^2+\omega^2}+\frac{\mu\eta_2\omega^2}{{\xi_2}^2+\omega^2}, \\ d_2 &= \frac{\rho\eta_1\xi_1}{{\xi_1}^2+\omega^2}+\frac{\mu\eta_2\xi_2}{{\xi_2}^2+\omega^2}. \end{aligned}$$

## 3. Stochastic averaging method

Substituting Eq. (5) into Eq. (12) gives the result

$$\begin{aligned} \dot{A} =\ & -c_3A^5\cos^4\varphi\sin^2\varphi+c_2A^3\cos^2\varphi\sin^2\varphi \\ & -(u_2+d_2-c_1)A\sin^2\varphi \\ & +\frac{(1+u_1+d_1)A\sin 2\varphi}{2\omega}+\frac{\varepsilon A^3\cos^3\varphi\sin\varphi}{\omega} \\ & -\frac{A\omega\sin 2\varphi}{2}-\frac{h\sin\varphi}{\omega}W(t), \\ \dot{\theta} =\ & -c_3A^4\cos^5\varphi\sin\varphi+c_2A^2\cos^3\varphi\sin\varphi \\ & -\frac{(u_2+d_2-c_1)\sin 2\varphi}{2} \\ & +\frac{(1+u_1+d_1)\cos^2\varphi}{\omega}+\frac{\varepsilon A^2\cos^4\varphi}{\omega} \\ & -\frac{\omega(1+\cos 2\varphi)}{2}-\frac{h\cos\varphi}{A\omega}W(t), \end{aligned} \tag{13}$$

where

$$\begin{aligned} u_1 &= \lambda_1\cos(\omega\tau)+\lambda_2\omega\sin(\omega\tau), \\ u_2 &= \lambda_2\cos(\omega\tau)-\frac{\lambda_1\sin(\omega\tau)}{\omega}, \\ d_1 &= \frac{\rho\eta_1\omega^2}{{\xi_1}^2+\omega^2}+\frac{\mu\eta_2\omega^2}{{\xi_2}^2+\omega^2}, \\ d_2 &= \frac{\rho\eta_1\xi_1}{{\xi_1}^2+\omega^2}+\frac{\mu\eta_2\xi_2}{{\xi_2}^2+\omega^2}. \end{aligned}$$

Based on the stochastic averaging method, we can derive the Itô differential equation of the amplitude $A$

$$\mathrm{d}A = m(A)\,\mathrm{d}t+\sigma(A)\,\mathrm{d}W(t). \tag{14}$$

Letting

$$\begin{aligned} F_1 =\ & -c_3A^5\cos^4\varphi\sin^2\varphi+c_2A^3\cos^2\varphi\sin^2\varphi \\ & -(u_2+d_2-c_1)A\sin^2\varphi \\ & +\frac{(1+u_1+d_1)A\sin 2\varphi}{2\omega} \\ & +\frac{\varepsilon A^3\cos^3\varphi\sin\varphi}{\omega}-\frac{A\omega\sin 2\varphi}{2}, \\ F_2 =\ & -c_3A^4\cos^5\varphi\sin\varphi+c_2A^2\cos^3\varphi\sin\varphi \\ & -\frac{(u_2+d_2-c_1)\sin 2\varphi}{2} \\ & +\frac{(1+u_1+d_1)\cos^2\varphi}{\omega} \\ & +\frac{\varepsilon A^2\cos^4\varphi}{\omega}-\frac{\omega(1+\cos 2\varphi)}{2}, \\ G_1 =\ & -\frac{h\sin\varphi}{\omega},\quad G_2 = -\frac{h\cos\varphi}{A\omega}, \end{aligned} \tag{15}$$

the average drift coefficient $m(A)$ and diffusion coefficient $\sigma(A)$ can be expressed as

$$\begin{aligned} m(A) &= \frac{1}{2\pi}\int_0^{2\pi}\left(F_1+G_1\frac{\partial G_1}{\partial A}D+G_2\frac{\partial G_1}{\partial\varphi}\frac{\partial\varphi}{\partial\theta}D\right)\mathrm{d}\varphi \\ &= -\frac{1}{16}c_3A^5+\frac{1}{8}c_2A^3-\frac{1}{2}A(u_2+d_2-c_1)+\frac{1}{2}\frac{h^2D}{A\omega^2}, \end{aligned}$$

$$\sigma^2(A) = \frac{D}{\pi}\int_0^{2\pi} G_1^2 \mathrm{d}\varphi = \frac{Dh^2}{\omega^2}. \tag{16}$$

Therefore, equation (14) can be written as

$$\begin{aligned}\mathrm{d}A =& -\frac{1}{16}c_3A^5 + \frac{1}{8}c_2A^3 - \frac{1}{2}A(u_2+d_2-c_1)\\ &+\frac{1}{2}\frac{h^2D}{A\omega^2}\mathrm{d}t + \frac{\sqrt{D}h}{\omega}\mathrm{d}W(t).\end{aligned} \tag{17}$$

in which

$$u_2 = \lambda_2\cos(\omega\tau) - \frac{\lambda_1\sin(\omega\tau)}{\omega},$$
$$d_2 = \frac{\rho\eta_1\xi_1}{{\xi_1}^2+\omega^2} + \frac{\mu\eta_2\xi_2}{{\xi_2}^2+\omega^2}.$$

The FPK equation related to Eq. (17) takes the following form:

$$\frac{\partial P(A,t)}{\partial t} = \frac{1}{2}\frac{\partial^2\left[\sigma^2(A)\cdot P(A,t)\right]}{\partial A^2} - \frac{\partial\left[m(A)\cdot P(A,t)\right]}{\partial A}. \tag{18}$$

The stationary probability density function of the amplitude $A$ can be obtained as

$$\begin{aligned}P(A) =& N^{-1}\cdot\frac{1}{\sigma^2(A)}\exp\left[\int\frac{2m(A)}{\sigma^2(A)}\mathrm{d}A\right]\\ =& N^{-1}\cdot A\exp\left[\frac{\omega^2}{Dh^2}\left(-\frac{1}{48}c_3A^6 + \frac{1}{16}c_2A^4\right.\right.\\ &\left.\left.-\frac{1}{2}(u_2+d_2-c_1)A^2\right)\right],\end{aligned} \tag{19}$$

where $N^{-1}$ is the normalized constant.

## 4. Discussion

### 4.1. Effectiveness of the method

In the goal to compare the analytical results obtained via the stochastic averaging method, the numerical simulation is made for the steady-state probability density functions of amplitude $A$, displacement $X$ and velocity $\dot{X}$. Fixed system parameters as: $h = 1.00$, $c_3 = 0.01$, $\varepsilon = 0.01$, $\lambda_1 = 0.01$, $\lambda_2 = 0.02$, $\rho = 0.05$, $\mu = 0.05$, $\eta_1 = 0.01$, $\eta_2 = 0.01$, $\xi_1 = 0.01$, $\xi_2 = 0.01$, $\omega = 1.00$. The solid lines represent analytical results obtained by the stochastic averaging method, and the discrete points are Monte Carlo numerical simulation results. Figures 2–5 show a good agreement between the analytical and numerical results. Therefore, the proposed method can maintain high precision.

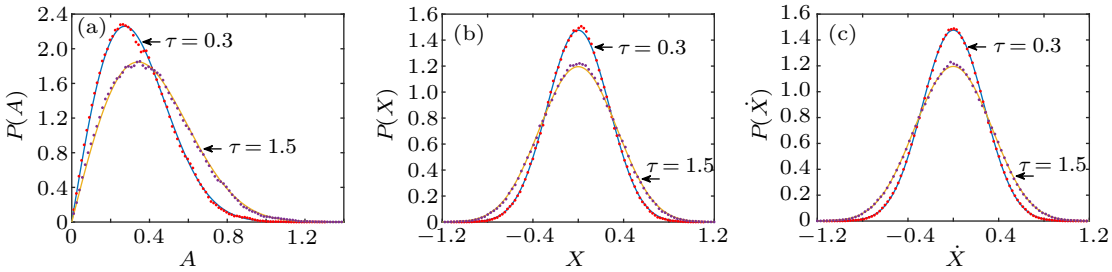



**Fig. 2.** Stationary probability density for two values of $\tau$ with $D = 0.005$, $c_1 = -0.05$, $c_2 = -0.05$: (a) amplitude $A$, (b) displacement $X$, (c) velocity $\dot{X}$.

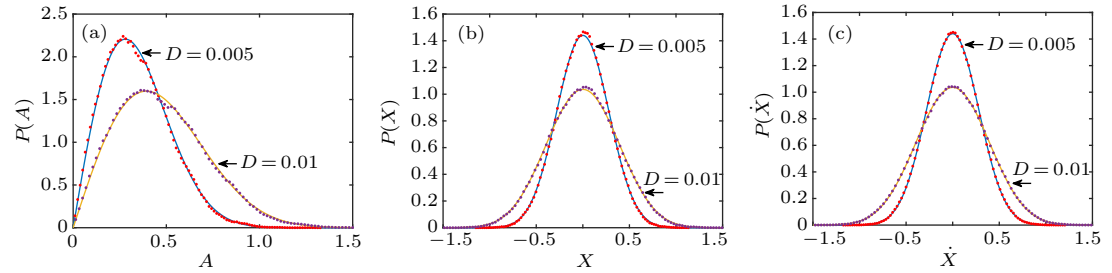



**Fig. 3.** Stationary probability density for two values of $D$ with $\tau = 0.5$, $c_1 = -0.05$, $c_2 = -0.05$: (a) amplitude $A$, (b) displacement $X$, (c) velocity $\dot{X}$.

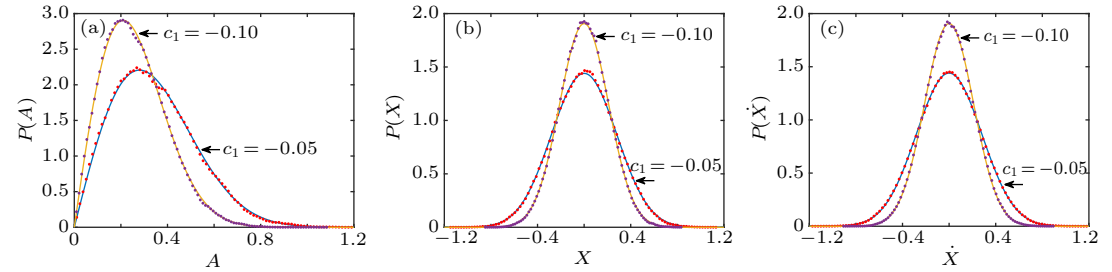



**Fig. 4.** Stationary probability density for two values of $c_1$ with $D = 0.005$, $\tau = 0.5$, $c_2 = -0.05$: (a) amplitude $A$, (b) displacement $X$, (c) velocity $\dot{X}$.

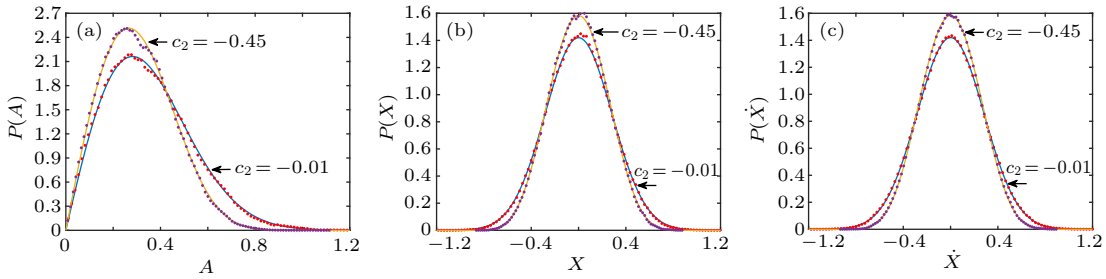



**Fig. 5.** Stationary probability density for two values of $c_2$ with $D = 0.005$, $\tau = 0.5$, $c_1 = -0.05$: (a) amplitude $A$, (b) displacement $X$, (c) velocity $\dot{X}$.

### 4.2. Stochastic *P*-bifurcation

Studying stochastic $P$-bifurcation can help design a more robust suspension system and reduce the risk of abnormal vibration induced by noise. A stochastic $P$-bifurcation occurs when the mode of the stationary probability density function changes, which represents a jump in the distribution of the random variable in a probabilistic sense.[56–58] This section focuses on judging the occurrence of stochastic $P$-bifurcation by single and double peak changes in the stationary probability density function. The critical conditions for the occurrence of $P$-bifurcation can be obtained from the following equation:[59]

$$\frac{\partial P(A)}{\partial A} = 0. \tag{20}$$

Substituting Eq. (19) into Eq. (20), we can obtain

$$\begin{aligned}\frac{\partial P(A)}{\partial A} = {} & N^{-1}\cdot\exp\left[\frac{\omega^2}{Dh^2}\left(-\frac{1}{48}c_3A^6+\frac{1}{16}c_2A^4\right.\right.\\ & \left.\left.-\frac{1}{2}(u_2+d_2-c_1)A^2\right)\right]\\ & \times\left[1+\frac{\omega^2}{Dh^2}\left[(c_1-u_2-d_2)A^2\right.\right.\\ & \left.\left.+\frac{1}{4}c_2A^4-\frac{1}{8}c_3A^6\right]\right],\end{aligned} \tag{21}$$

let $\partial P(A)/\partial A = 0$, the following expression can be obtained:

$$1+\frac{\omega^2}{Dh^2}\left[(c_1-u_2-d_2)A^2+\frac{1}{4}c_2A^4-\frac{1}{8}c_3A^6\right]=0, \tag{22}$$

where

$$\begin{aligned}u_2 &= \lambda_2\cos(\omega\tau)-\frac{\lambda_1\sin(\omega\tau)}{\omega},\\ d_2 &= \frac{\rho\eta_1\xi_1}{{\xi_1}^2+\omega^2}+\frac{\mu\eta_2\xi_2}{{\xi_2}^2+\omega^2}.\end{aligned}$$

The boundary curves $B_1$ and $B_2$ obtained from Eq. (22) divide the system parameter plane into two parts: regions $S_1$ and $S_2$. The points in region $S_1$ correspond to the steady-state probability density function of one peak, and the points in region $S_2$ correspond to the steady-state probability density function of two peaks. Fixed system parameters as: $h = 1.00$, $\varepsilon = 0.01$, $\lambda_1 = 0.01$, $\lambda_2 = 0.02$, $\rho = 0.05$, $\mu = 0.05$, $\eta_1 = 0.01$, $\eta_2 = 0.01$, $\xi_1 = 0.01$, $\xi_2 = 0.01$, $\omega = 1.00$.

Firstly, figure 6(a) shows that regions $S_1$ and $S_2$ in the $(c_1, D)$ plane are delineated by the boundaries $B_1$ and $B_2$, and the structure of the steady-state probability density function is unimodal and bimodal in the $S_1$ and $S_2$ regions, respectively. Select these points $(-0.30, 0.2)$, $(-0.15, 0.2)$, $(-0.05, 0.2)$ in the parameter plane and mark these points with a red five-pointed star. The graphical representation of steady-state probability density functions for points in Fig. 6(b) shows their nature. Obviously, the stationary probability density functions of $(-0.30, 0.2)$, $(-0.05, 0.2) \in S_1$ are unimodal, while that of $(-0.15, 0.2) \in S_2$ is bimodal. This shows that as $c_1$ increases from $-0.30$ to $-0.05$, the shape of the steady-state probability density function changes from unimodal to bimodal and back again. It implies that the variation of system parameter $c_1$ causes stochastic $P$-bifurcation.

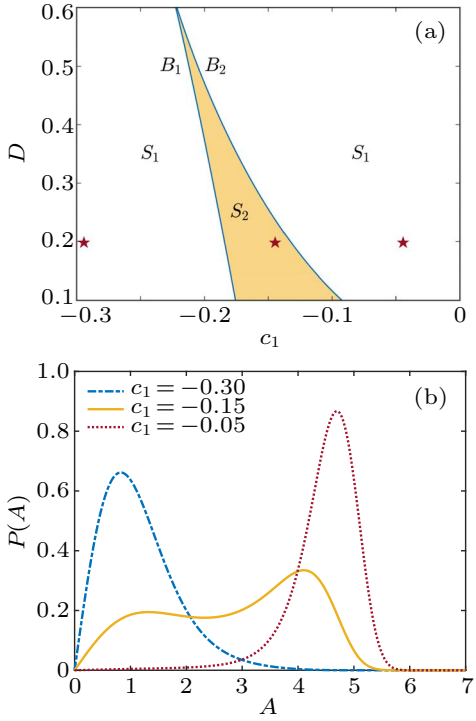



**Fig. 6.** The parameter plane $(c_1, D)$ with $c_2 = 0.12$, $c_3 = 0.01$, $\tau = 0.5$: (a) Bifurcation diagram, (b) stationary probability density of amplitude $A$ for three values of $c_1$.

Secondly, figures 7(a) and 6(a) depict the same parameter plane, but figure 7(a) selects parameter points $(-0.185, 0.12)$, $(-0.185, 0.3)$, $(-0.185, 0.59)$. The steady-state probability

density function images corresponding to the parameter points are drawn in Fig. 7(b). We can know that the stationary probability density function of $(-0.185, 0.12)$ and $(-0.185, 0.59) \in S_1$ is unimodal, while the stationary probability density function of $(-0.185, 0.3) \in S_2$ is bimodal. The analysis reveals a $D$-dependent modal transition in the stationary probability density function exhibiting sequential unimodal–bimodal–unimodal characteristics with increasing $D$. This shows that the change of system parameter $D$ induces the occurrence of stochastic $P$-bifurcation.

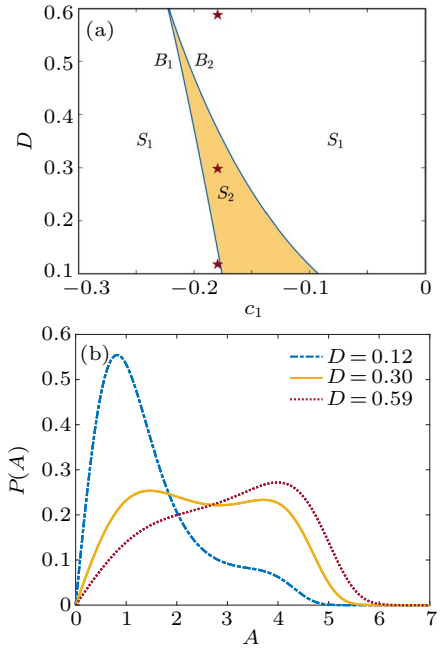



**Fig. 7.** The parameter plane $(c_1, D)$ with $c_2 = 0.12$, $c_3 = 0.01$, $\tau = 0.5$: (a) bifurcation diagram, (b) stationary probability density of amplitude $A$ for three values of $D$.

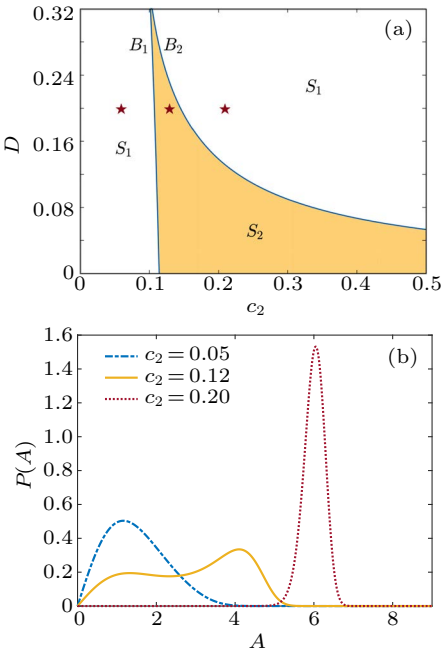



**Fig. 8.** The parameter plane $(c_2, D)$ with $c_1 = -0.15$, $c_3 = 0.01$, $\tau = 0.5$: (a) bifurcation diagram, (b) Stationary probability density of amplitude $A$ for three values of $c_2$.

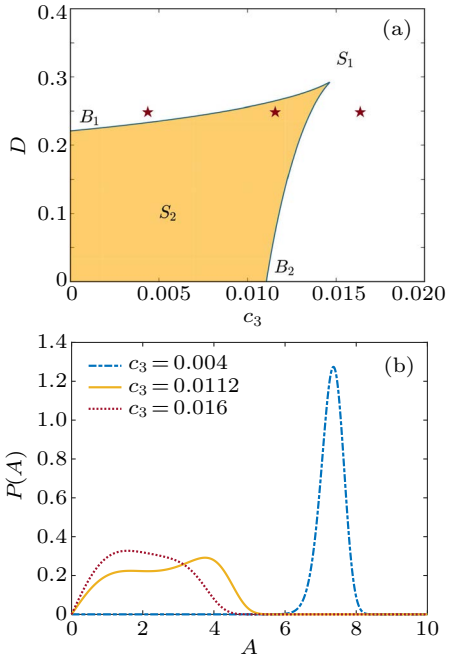



**Fig. 9.** The parameter plane $(c_3, D)$ with $c_1 = -0.15$, $c_2 = 0.12$, $\tau = 0.5$: (a) bifurcation diagram, (b) stationary probability density of amplitude $A$ for three values of $c_3$.

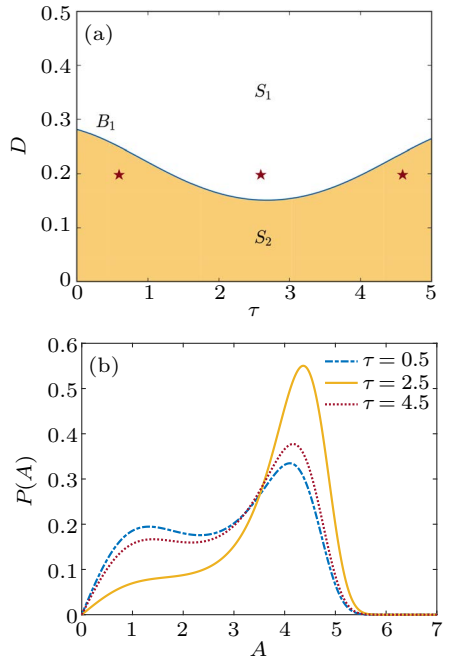



**Fig. 10.** The parameter plane $(\tau, D)$ with $c_1 = -0.15$, $c_2 = 0.12$, $c_3 = 0.01$: (a) bifurcation diagram, (b) stationary probability density of amplitude $A$ for three values of $\tau$.

Third, figures 8(a) and 9(a) are stochastic $P$-bifurcation diagrams of the parameter planes $(c_2, D)$ and $(c_3, D)$, respectively. Figure 8(b) depicts the probability density function image have a unimodal-bimodal-unimodal transition with $c_2$ increasing from 0.05 to 0.2. As can be seen from Fig. 9(b), when $c_3$ increases from 0.004 to 0.016, the corresponding steady-state probability density function changes from unimodal to bimodal and back to unimodal. The above interpretation of Figs. 8 and 9 depicts that stochastic $P$-bifurcation appears accompanying the variation of parameters $c_2$ and $c_3$.

Finally, the stochastic $P$-bifurcation diagram induced by time delay $\tau$ and noise intensity $D$ is shown in Fig. 10(a). The points $(0.5,0.2)$ and $(4.5,0.2) \in S_2$, $(2.5,0.2) \in S_1$ are selected from the parameter plane $(\tau, D)$, and the corresponding probability density function images are shown in Fig. 10(b). From the observation of the images, it can be seen that the steady-state probability density function of the amplitude $A$ suffers a change from single peak shape to the shape of the twin peaks and back to single peak shape when $\tau$ changes from 0.5 to 4.5. The analysis reveals that modifying the time delay $\tau$ can cause stochastic $P$-bifurcation to occur.

### 4.3. Analysis of system performance

This section mainly discuss the effect of some important parameters on the system energy recovery performance. Fixed system parameters as: $h = 1.00$, $c_3 = 0.01$, $c_2 = -0.05$, $c_1 = -0.05$, $\varepsilon = 0.01$, $\lambda_1 = 0.01$, $\lambda_2 = 0.02$, $\rho = 0.05$, $\eta_1 = 0.01$, $\xi_1 = 0.01$. Figures 11 and 12 reveal how the mean output power changes as system parameters change.

Based on Eqs. (11a) and (11b), in stationary conditions, the current and voltage take the following form:

$$I_0 = \frac{\eta_1 \omega}{\sqrt{\xi_1^2 + \omega^2}} A \quad V_0 = \frac{\eta_2 \omega}{\sqrt{\xi_2^2 + \omega^2}} A. \tag{23}$$

As derived in Eq. (23), the mean squared current and voltage take the form

$$E[I^2] = E[I_0^2] = \frac{\eta_1^2 \omega^2}{\xi_1^2 + \omega^2} \int_0^{+\infty} A^2 P(A)\,\mathrm{d}A,$$
$$E[V^2] = E[V_0^2] = \frac{\eta_2^2 \omega^2}{\xi_2^2 + \omega^2} \int_0^{+\infty} A^2 P(A)\,\mathrm{d}A. \tag{24}$$

The average harvested power can be expressed as

$$E[P] = E[P_I] + E[P_V] = \rho \xi_1 E[I^2] + \mu \xi_2 E[V^2]. \tag{25}$$

Figure 11 shows the influence of system parameters $\eta_2$, $\xi_2$, and $\mu$ on the mean output power under different noise intensity $D$. As can be seen from Fig. 11, the mean output power increases with the increase of parameters $D$, $\eta_2$, $\mu$, while the mean output power increases first and then decreases slightly with the increase of parameter $\xi_2$.

Figure 12 depicts the effect of system parameters $\eta_2$, $\xi_2$, and $\mu$ on the mean output power for different values of time delay $\tau$. It can be observed from Fig. 12 that the mean output power increases with the increase of parameters $\eta_2$ and $\mu$, while as parameter $\xi_2$ increases, the mean output power increases first and then decreases slightly. In addition, time delay $\tau$ from 0.5 to 1.0 and then to 1.5, the mean output power first increases and then decreases.

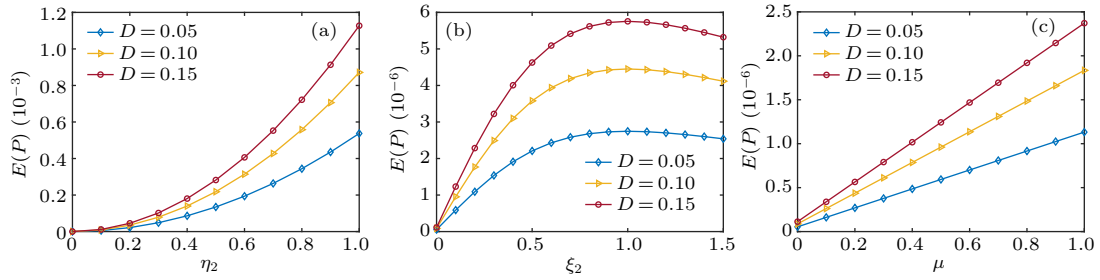



**Fig. 11.** The mean output power $E(P)$ varies with system parameters under different noise intensity $D$: (a) $\eta_2$ ($\xi_2 = 0.01$, $\mu = 0.05$, $\tau = 0.5$, $\omega = 1.00$), (b) $\xi_2$ ($\eta_2 = 0.01$, $\mu = 0.05$, $\tau = 0.5$, $\omega = 1.00$), (c) $\mu$ ($\eta_2 = 0.01$, $\xi_2 = 0.05$, $\tau = 0.5$, $\omega = 1.00$).

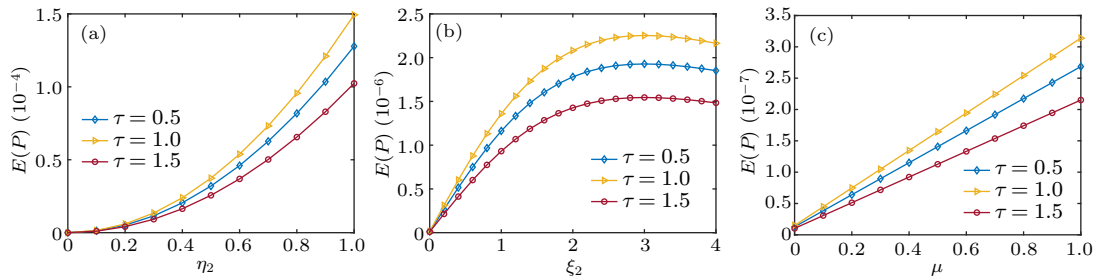



**Fig. 12.** The mean output power $E(P)$ varies with system parameters under different time delay $\tau$: (a) $\eta_2$ ($\xi_2 = 0.01$, $\mu = 0.05$, $D = 0.05$, $\omega = 3.00$), (b) $\xi_2$ ($\eta_2 = 0.01$, $\mu = 0.05$, $D = 0.05$, $\omega = 3.00$), (c) $\mu$ ($\eta_2 = 0.01$, $\xi_2 = 0.05$, $D = 0.05$, $\omega = 3.00$).

## 5. Conclusions

In this paper, the probability distribution and $P$-bifurcation of a nonlinear energy-regenerative suspension system with time delay were investigated. In the beginning, mathematical model with approximate equivalent was derived through conversion of the time delay, electrical parameters (current and voltage) into mechanical terms (displacement and velocity). Then the steady-state probability density function of the amplitude was obtained by using stochastic averaging method. Thirdly, the analytical solutions of steady-state

probability density functions of amplitude, displacement and velocity agreed well with the numerical solutions simulated by Monte Carlo method, which verified the validity of the stochastic averaging method. In the end, how the system parameters affect the stochastic *P*-bifurcation and the average output power was analyzed and some conclusions were obtained.

By drawing the bifurcation diagram of the parameter plane and the corresponding probability density function images, it indicates that the changes in damping coefficient, noise intensity and time delay can lead to stochastic *P*-bifurcation. And then proceeds to discuss how the time delay, noise intensity, and electromechanical coupling coefficient affect the average output power. It was revealed that the average output power increases first and then decreases at any time in a period, the mean output power exhibits a positive correlation with both noise intensity and the electromechanical coupling coefficient.

The findings of this study establish a theoretical foundation for initial design considerations and parameter optimization in energy-regenerative suspension incorporating both piezoelectric and electromagnetic transduction.

## Acknowledgements

Project supported by the National Natural Science Foundation of China (Grant No. 12002089), the Science and Technology Projects in Guangzhou (Grant No. 2023A04J1323), and UKRI Horizon Europe Guarantee (Marie Skłodowska-Curie Fellowship) (Grant No. EP/Y016130/1).

## References

[1] Kasseris E P and Heywood J B 2007 *SAE Transactions* 626
[2] Wang R, Chen Z, Xu H, Schmidt K, Gu F and Ball A D 2014 *IEEE Proceedings of* 20*th International Conference on Automation and Computing* p. 32
[3] Fan Y and Sun J 2017 *Mechanics* **23** 92
[4] Hrovat D 1997 *Automatica* **33** 1781
[5] Abdelkareem M A, Makrahy M M, Abd-El-Tawwab A M, El-Razaz A, Kamal Ahmed Ali M and Moheyeldein M 2018 *Proceedings of the Institution of Mechanical Engineers, Part K: Journal of Multi-body Dynamics* **232** 84
[6] Rana R S and Adhyaru D M 2023 *Journal of Circuits, Systems and Computers* **32** 2350312
[7] Kim H J, Kang S M, Kim S M and Kim J H 2024 *International Journal of Automotive Technology* **25** 627
[8] Wang H, Jasim A and Chen X 2018 *Applied Energy* **212** 1083
[9] Ali M K A, Fuming P, Younus H A, Abdelkareem M A, Essa F, Elagouz A and He X J 2018 *Applied Energy* **211** 461
[10] Wei C and Jing X 2017 *A Renewable and Sustainable Energy Reviews* **74** 1
[11] Rehman A U, Ryu S W, Park H and Jung J W 2024 *IEEE Transactions on Industrial Informatics* **20** 6060
[12] Sun Y H, Zeng Z B and Huang M L 2024 *Engineering Structures* **312** 118211
[13] Abdelkareem M A, Xu L, Guo X, Ali M K A, Elagouz A, Hassan M A, Essa F and Zou J 2018 *Mechanical Systems and Signal Processing* **110** 307
[14] Guan Y, Li W, Kozak D and Zhao J 2024 *Reliability Engineering & System Safety* **249** 110206
[15] Huang D, Han J, Li W, Deng H and Zhou S 2023 *Commun. Nonlinear Sci. Numer. Simul.* **119** 107086
[16] Liang Q, Yu W X and Xiao Q M 2025 *Chin. Phys. B* **34** 040502
[17] Han J, Huang D, Li W, Yang G and Gubeljak N 2023 *International Journal of NonLinear Mechanics* **157** 104518
[18] Khoshnoud F, Zhang Y, Shimura R, Shahba A, Jin G, Pissanidis G, Chen Y K and De Silva C W 2015 *IEEEASME Transactions on Mechatronics* **20** 2513
[19] Cui T H, Li J, Yuan Q, Wei Y Q, Dai S Q, Li P D, Zhou F, Zhang J Q, Chen L and Feng M 2023 *Chin. Phys. Lett.* **40** 080501
[20] Huang B, Hsieh C Y, Golnaraghi F and Moallem M 2015 *Journal of Sound and Vibration* **357** 16
[21] Wei C and Taghavifar H 2017 *Energy* **134** 279
[22] Zhang H, Guo X, Fang Z, Xu L and Zhang J 2015 *Journal of Vibration, Measurement & Diagnosis* **35** 225
[23] Wang R, Gu F, Cattley R and Ball A D 2016 *Energies* **9** 386
[24] Zou J, Guo X, Abdelkareem M A, Xu L and Zhang J 2019 *Mechanical Systems and Signal Processing* **127** 345
[25] Liang H, Hao G and Olszewski O Z 2021 *Sensors and Actuators A: Physical* **331** 112743
[26] Ibrahim P, Arafa M and Anis Y 2021 *Sensors* **21** 5611
[27] Wang M, Yin P, Li Z, Sun Y, Ding J, Luo J, Xie S, Peng Y and Pu H 2020 *Energy Conversion and Management* **220** 113050
[28] Zhao Z, Wang T, Zhang B, Shi J, *et al.* 2015 *Mathematical Problems in Engineering* **2019** 1
[29] Xie X and Wang Q 2015 *Energy* **86** 385
[30] Xiao H, Wang X and John S 2015 *Mechanical Systems and Signal Processing* **58** 355
[31] Kou F, Jing Q, Chen C and Wu J 2020 *Shock and Vibration* **2020** 1
[32] Zuo L, Scully B, Shestani J and Zhou Y 2010 *Smart Materials and Structures* **19** 045003
[33] Li C and Peter W T 2013 *Smart Materials and Structures* **22** 065024
[34] Zhang J, Liu J, Liu B and Li M 2022 *Actuators* **11** 189
[35] Suda Y and Shiiba T 1996 *Vehicle System Dynamics* **25** 641
[36] Zhang Z, Zhang X, Chen W, Rasim Y, Salman W, Pan H, Yuan Y and Wang C 2016 *Applied Energy* **178** 177
[37] Liu Y, Xu L and Zuo L 2017 *IEEEASME Transactions on Mechatronics* **22** 1933
[38] Satpute N, Iwaniec M, Narina R and Satpute S 2020 *Vibrations in Physical Systems* **31**
[39] Taghavifar H 2021 *Mechanical Systems and Signal Processing* **146** 106988
[40] Gu K and Niculescu S I 2003 *Journal of Dynamic Systems, Measurement, and Control* **125** 158
[41] Wang Q, Wu H and Yang Y 2022 Nonlinear Dynamics 1
[42] Cermák C and Nechvátal L 2020 *Physica D* **404** 132339
[43] Belhaq M, Ghouli Z and Hamdi M 2018 *Nonlinear Dynamics* **94** 2537
[44] Sun X, Xu J and Fu J 2017 *Mechanical Systems and Signal Processing* **87** 206
[45] Yang T and Cao Q 2019 *Nonlinear Dyn.* **96** 1511
[46] Jin Y and Meng J 2020 *Commun. Nonlinear Sci. Numer. Simul.* **90** 105333
[47] Zhang Y, Jin Y and Li Y 2021 *Physica D* **422** 132908
[48] Wu K, Ren C and Atay F M 2024 *Energy* **300** 131578
[49] Hamdi M and Belhaq M 2018 *Recent Trends in Applied Nonlinear Mechanics and Physics* pp. 69–83
[50] Nguyen C H, Nguyen D S and Halvorsen E 2014 *J. Phys.: Conf. Ser.* **557** 012114
[51] Fokou I M, Buckjohn C N D, Siewe M S and Tchawoua C 2018 *Commun. Nonlinear Sci. Numer. Simul.* **56** 177
[52] Stratonovich R L 1967 *Topics in the Theory of Random Noise*, Vol. 2 (CRC Press)
[53] Zhu W 1996 *Applied Mechanics Reviews* **49** S72
[54] Guan Y, Li W, Huang D and Gubeljak N 2023 *Chaos, Solitons and Fractals* **173** 113641
[55] Yang Y G, Huang M L, Guo S L and Sun Y H 2023 *Mechanical Systems and Signal Processing* **186** 109837
[56] Yang J, Sanjuán M A, Liu H, Litak G and Li X 2016 *Commun. Nonlinear Sci. Numer. Simul.* **41** 104
[57] Wang R, Ding Y and Kang Y 2024 *The European Physical Journal Special Topics* 1
[58] Sun Y H, Sun Y, Yang Y G and Xu W 2023 *Probabilistic Engineering Mechanics* **73** 103464
[59] Liao Z J, Sun Y H and Liu Y 2024 *Chin. Phys. B* **33** 070205